Journal of
Bioengineering & Biomedical Science

Ledesma-Carrión, J Bioengineer & Biomedical Sci 2016, 6:3
DOI: 10.4172/2155-9538.1000189

Research Article Open Access

Characterization and Effect of Anatase on Nano- Hydroxyapatite

Dora E. Ledesma-Carrión*

National Institute of Statistic and Geography, C.P. 03730 Delg, Benito Juárez, Mexico

Abstract

The main bone substitute is hydroxyapatite either mineral or synthetic. Synthetic hydroxyapatite is produced by various methods such as, sol-gel, mechanochemical, hydrothermal, sonochemical, ceramic (wet and dry roads, routes through cements of calcium phosphates and route using emulsions-microemulsions), and hydrolysis. Hydroxyapatite obtained by wet via has features from micro to nano. It has been reported that adding titania mechanical properties of hydroxyapatite improve. In this study only the experimental evidence is presented. The objective of this study was to analyze the effect of anatase in synthetic hydroxyapatite obtained by co-precipitators. Powders were subjected to uniaxial and isostatic cold pressing to form pills. Later pills were sintered. The characterization of the material includes several techniques. It was compared with each of the different percentages of anatase 0.1, 1.5, 1, 3, 5, 7 and 10. The results show the existence of an optimum percentage by which the mechanical properties surpass others, maximum of hardness before immersed it in simulated body fluid with 7%. The explanation of this optimum is the presence of calcium titanate because of titania diffuses efficiently in the network hydroxyapatite.

Keywords: Bond; Nanostructure; Hydroxyapatite; Characterization; Particle size; Anatase; Hardness

Abbreviations: SEM-EDS: Energy-dispersive X-ray Spectroscopy; SEM-HR: Scanning Electron Microscopy of High-resolution; TEM-HR: Transmission Electron Microscopy of High-resolution; TEM: Transmission Electron Microscopy; TGA: Thermogravimetric Analysis; DSC: Differential Scanning Calorimetry; BET: Surface adsorption tests due to Brunauer–Emmett–Teller (BET) Theory; BJH: Surface Adsorption tests due to Barrett-Joyner-Halenda; SBF: Simulated Body Fluid; UP: Uniaxial Pressure; CIP: Cold Isostatic Pressure; FT-IR: Fourier Transform Infrared Spectroscopy; XPS: X-ray Photoelectron Spectroscopy; XDR: X-ray Diffraction; HA: Hydroxyapatite; HA sc: Hydroxyapatite Powder without Heat Treatment; HA cc: Hydroxyapatite Powder with Heat Treatment; Ar: Argon; HA90cc: 90%HAcc+10%TiO_2; HA93cc: 93%HAcc+7%TiO_2; HA95cc: 95%HAcc+5%TiO_2; HA97cc: 97%HAcc+3%TiO_2; HA99cc: 99%HAcc+1%TiO_2; HA99.9cc: 99.9%HAcc+0.1%TiO_2

Introduction

Studies have shown that microcrystalline HA is known as a substitute "good-builder" with higher calcium absorption. It is a charge of second-generation calcium derived from bovine bone. And it is more effective than calcium carbonate in slow bone loss [1,2].

The composition of the mineral HA stoichiometric be expressed as Ca_{10} (PO_4) 6 $(OH)_2$ with a Ca / P = 1.67 relationship, while the HA deficient in calcium (CDHA) is CA_9 (HPO_4) (PO_4) 5 (OH), with Ca / P = 1.50. The latter is the one that is considered the most similar to human bones [3].

Biocompatibility tests [4,5] natural HA (bovine base) and titanium dioxide show regeneration and capillarity after a few weeks.

Nanometric and stoichiometric hydroxyapatite was prepared by wet via [6]. Later, TiO_2 anatase was added. The analysis was made on powder with heat treatment at 680°C in Ar atmosphere (HA cc) and pills. The powders were subjected to UP and CIP to form pills [7]. The pills %HAcc+%TiO_2 were sintered at 850°C. HA cc and TiO_2 median size were 175.9 and 293.6 nm, respectively. Using other technique, Kumar et al. [8] reported hardness and elasticity of 15.1 and 0.405 GPa by nano-indentation for a load of 100 mN over a coating of subsequent layers of %HA%TiO_2 (25%HA75%TiO_2, 50%HA50%TiO_2, 75%HA25%TiO_2 and HA). These layers were sintered at 900°C during a few minutes with functionally graded successfully. Before, HA was calcined at 800°C for 2 h. HA and TiO_2 median size are 7.46 and 1.37 µm, respectively.

Fidancevska et al. [9] mixed HA and titanium powder to produce porous bionert-bioactive composite ceramic and reported an optimum value at 15wt. % of TiO_2 but at 20wt. % the Young modulus decreased, the median size HA was 5 µm. This was the first evidence of an optimum value at micrometer particles.

Materials and Methods

The characterization of the material includes SEM-HR, TEM, TEM-HR, FTIR, Raman, TGA / DSC, XRD, BET / BJH, XPS, nano-indentation and Z-sizer.

Figures 1 and 2a show anatase and rutile phases of TiO_2 and amorphous and crystalline HA sc in air, therefore inert atmosphere (Ar) must be used and not exceed the heat treatment of 680°C and sintering of 850°C. Upon heating in air, phosphates and carbonates appear in HA sc at 980°C and 630°C, respectively, Figure 2b. Thus, to obtain calcium titanate instead of calcium carbonate should control the rate of calcination and the atmosphere.

Micrographs increased x75000, SEM 10KV and 93.3pA. PANalytical XPert PRO (45KV, 40mA) was used. XPS k-alpha: Al-Kα 1486.6 eV and 10-8 mbars. Raman at 633 cm^{-1}. UP No. 714987 RAM DIA 600. Dade diameter was 1cm of steel 316L. CIP was made with a Yuken Model 334 press applied 400MPa during one cycle of four steps: Step 1: 0-100MPa, step 2: 101-200MPa, step 3: 201-300MPa and step 4:

***Corresponding author:** Dora E. Ledesma-Carrión, National Institute of Statistic and Geography, C.P. 03730 Delg, Benito Juárez, Mexico, Tel: 525552781000; E-mail: ged_62@yahoo.com

Received: May 04, 2016; **Accepted:** May 19, 2016; **Published**: May 30, 2016

Citation: Ledesma-Carrión DE (2016) Characterization and Effect of Anatase on Nano- Hydroxyapatite. J Bioengineer & Biomedical Sci 6: 189. doi:10.4172/2155-9538.1000189

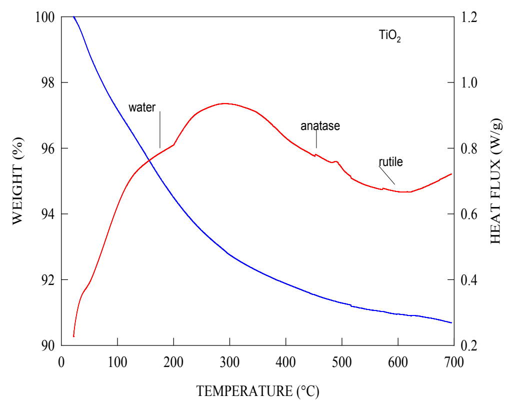

Figure 1: TGA/DSC test: Phases of TiO_2, anatase and rutile, are observed at 480°C and 580°C, respectively.

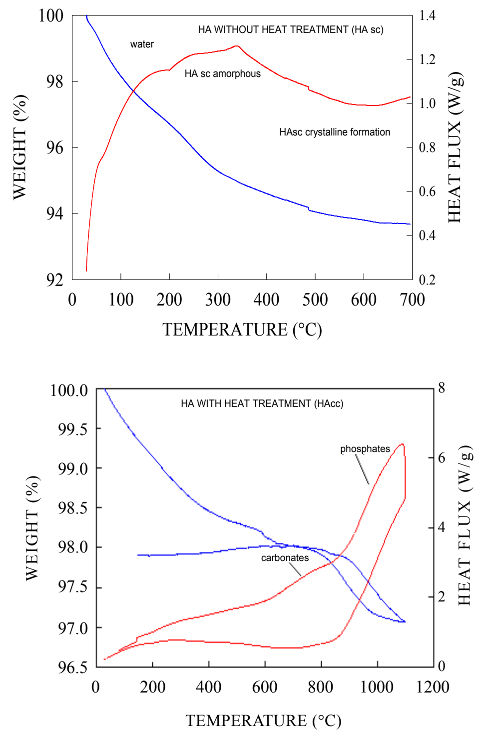

Figure 2: TGA/DSC test: a) HAsc begins to crystallize at 475°C and b) HAcc which one is crystalline and break down in carbonates and phosphates at 700°C and 900°C, respectively.

301-400MPa. Time of step is 30 seconds. After the pills were sintered at 850°C in Ar atmosphere since 500°C during 1hr, heat up slop 5°C /min and heat slope down 6°C /min. Fourteen zones were studied for each pill after immerged in SBF. The SBF was made following the method of Oyane et al. [10].

Results and Discussion

Figure 3 show TGA curves for different percentages of anatase. For HA95cc is observed the lower area of carbonates and for most HA90cc. Comparing heat capacities, Cp´s for %HAcc + %TiO_2 are showed in Figure 4. The Cp´s for HA95cc are analogous to that of anatase in the

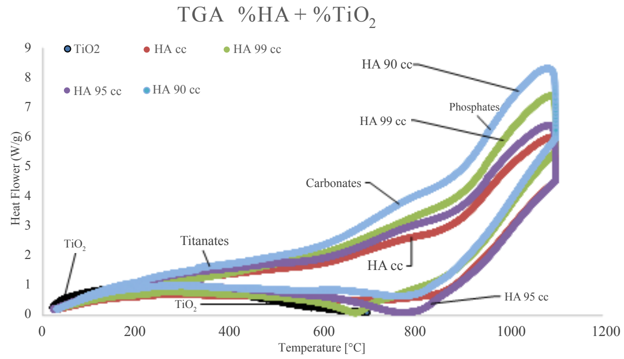

Figure 3: TGA tests %HAcc + %TiO_2 show same carbonate and phosphates zones for each percentage of dioxide of titanium.

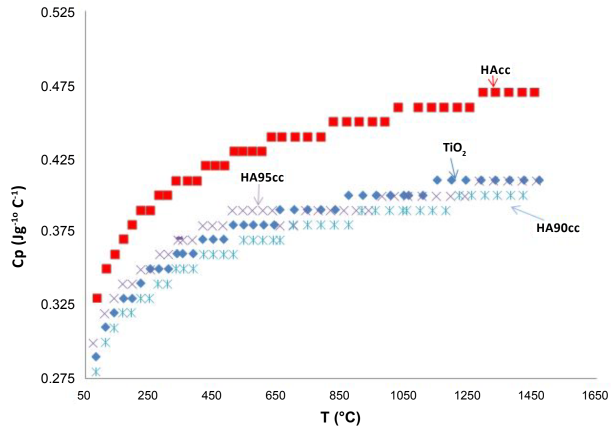

Figure 4: %HAcc + %TiO_2 calorific capacities, Cps, show similar values into some ranges with anatase.

following ranges: (751.717°C, 833.001°C; Cp = 0.389853 J $Jg^{-1o}C^{-1}$), (968.258°C, 1107.09°C; Cp = 0.400155 $Jg^{-1o}C^{-1}$) and (1276.49°C, 1445.88°C; Cp = 0.410457 $Jg^{-1o}C^{-1}$). X-ray diffraction patterns do not present CaO, see Figures 5 and 6, but show titanato ion, TiO^{-3}_2. The peak area is significant from HA95cc up to HA90cc.

To verify pore size in a nanometer range in Figure 7 and Tables 1 and 2 appear Nitrogen-Adsorption-desorption (BET/BJH) tests. Those showed mesoporosity with a maximum area reduction of 8.93% and maximum pore radii of 1.88 nm for HA95.

And particles average size distribution, Figure 8 shows that for anatase is 294nm, HAcc is 175.9nm, HA95cc is 293.6nm and HA90cc is 206.4nm. The 2-modal distribution for HA95cc is evidence of the spread of titania in the HAcc. The tetragonal crystalline structure of HA95cc and HA90cc is observed in the Figure 9. The anatase structure is tetragonal and HAcc is hexagonal, Figure 10, is expected that %HAcc+%TiO_2 are tetragonal. The morphology change is followed in Figure 11. The anatase into "balls" surrounding the cylindrical bars HAcc. This balance is in HA95cc and HA93cc.

Raman spectra show titanate ion together υ_3 anatase, and characteristic picks HAcc, Figure 12. TiO_2 [11,12] υ_1 absorption band appears at 600-700cm^{-1} and 525-460cm^{-1}. υ_2 band is at 380-329cm^{-1}

Citation: Ledesma-Carrión DE (2016) Characterization and Effect of Anatase on Nano- Hydroxyapatite. J Bioengineer & Biomedical Sci 6: 189. doi:10.4172/2155-9538.1000189

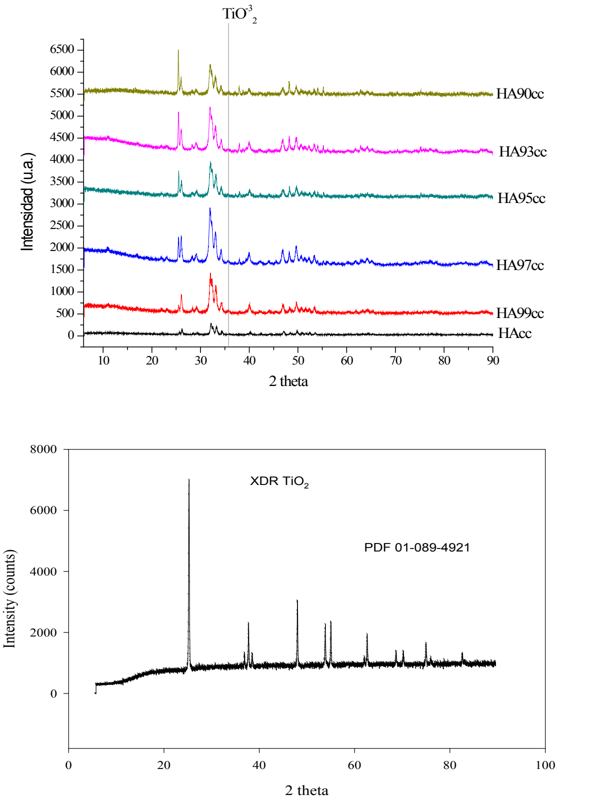

Figure 5: %HAcc+%TiO_2 XRD pattern without CaO plane but TiO^{-3}_2 pick.

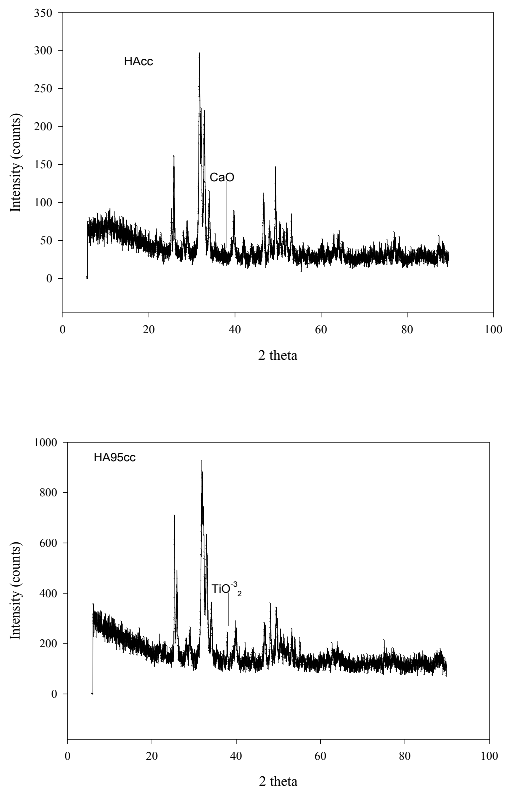

Figure 6: HAcc and HA95cc diffraction patters do not observe CaO plane or rutile phase. And TiO^{-3}_2 pick.

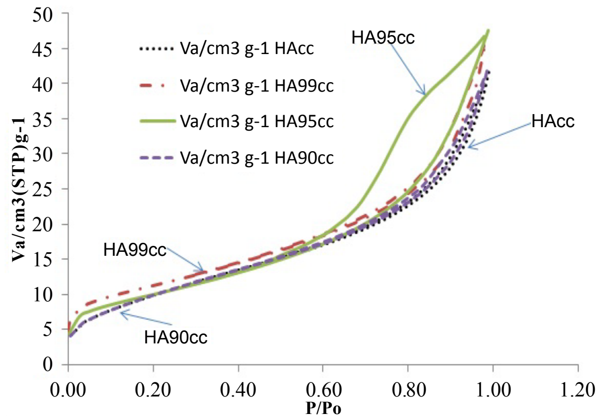

Figure 7: BET tests %HAcc + %TiO_2 show mesoporosity for each percentage of dioxide of titanium. The smallest porosity is in 5%TiO_2.

BET Analysis %HAcc + %TiO_2		
sample	area [m²/g]	
Hacc 100%	37.8	
Hacc 99%TiO_2 1%	37.9	0.26%
Hacc 95%TiO_2 5%	34.7	-8.44%
Hacc 90%TiO_2 10%	37.8	8.93%

Table 1: %HAcc + %TiO_2 BET tests show reduced total area.

Plot data	100%HAcc	Adsorption branch
V_p		0.061055 [cm³ g⁻¹]
$r_{p,peak}$(Area)		1.22 [nm]
a_p		32.53 [m² g⁻¹]
Plot data	99%HAcc+1%TiO_2	Adsorption branch
V_p		0.064385 [cm³ g⁻¹]
$r_{p,peak}$(Area)		1.66 [nm]
a_p		30.429 [m² g⁻¹]
Plot data	95%HAcc+5%TiO_2	Adsorption branch
V_p		0.069464 [cm3 g⁻¹]
$r_{p,peak}$(Area)		1.88 [nm]
a_p		31.243 [m² g⁻¹]
Plot data	90%HAcc+10%TiO_2	Adsorption branch
V_p		0.060931 [cm³ g⁻¹]
$r_{p,peak}$(Area)		1.22 [nm]
a_p		33.404 [m² g⁻¹]

Table 2: %HAcc + %TiO_2 BJH tests show pore volumen, peak radii and area.

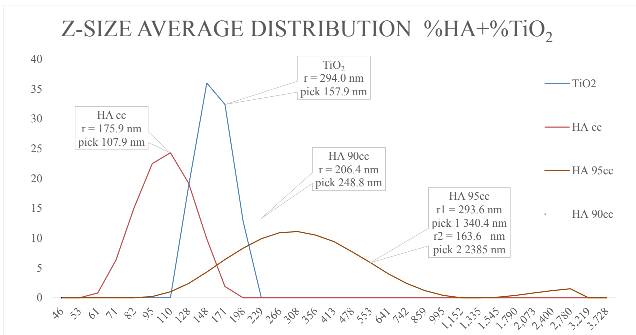

Figure 8: Z-Size Average Distributions show 1-modal forms for HAcc, HA90cc and TiO_2, and 2-modal for HA95cc.

Citation: Ledesma-Carrión DE (2016) Characterization and Effect of Anatase on Nano- Hydroxyapatite. J Bioengineer & Biomedical Sci 6: 189. doi:10.4172/2155-9538.1000189

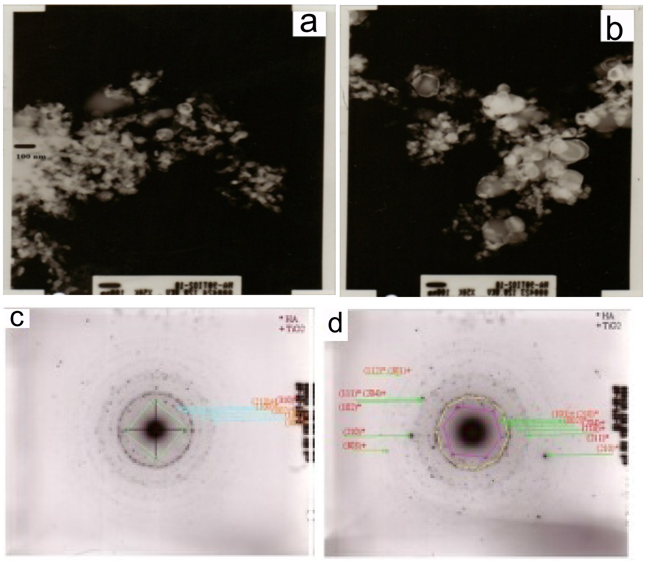

Figure 9: Electron diffraction pattern a) HA95cc TEM micrograph shows nanostructure ~100nm, b) HA90cc TEM micrograph shows particle size ~200nm. Electron diffraction shows nanostructure and lightly textured for, c) HA95cc and d) HA90cc.

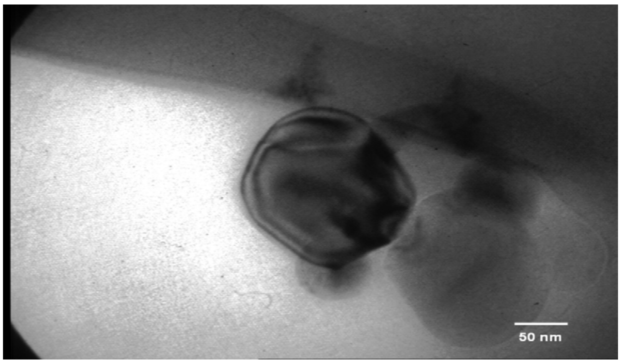

Figure 10: HAcc TEM-HR micrograph shows hexagonal nanostructure and particle size ~100nm.

and υ_3 band is at 185-91cm^{-1} and 100-91cm^{-1}. The FTIR is more specific, they show the change of carbonates and phosphates to calcium titanate. The FTIR experiments were not made in Ar atmosphere but in air, Figure 13.

XPS tests show electrons 2p of titanium replace 2p electrons of phosphorus to bind calcium, see Figure 14. It shows 2p Ca (347.5eV, 351.5eV), 1s O (530.5-531eV), 2p Ti (459.5eV), 2p P (132.5eV) and hydroxyl (531-532eV) bonding energy. For Tables 3 and 4, maximum hardness and elasticity are at HA93cc before SBF. They are minimums after 1 day into SBF. The maximum work of elasticity and plasticity are HA93cc after SBF. The total work increases 52%.

Conclusion

This optimal is between 5wt%TiO_2 and 7wt%TiO_2. The process favors the formation of calcium titanate bond. It is important to produce hydroxyapatite without carbonates for titanium take its place

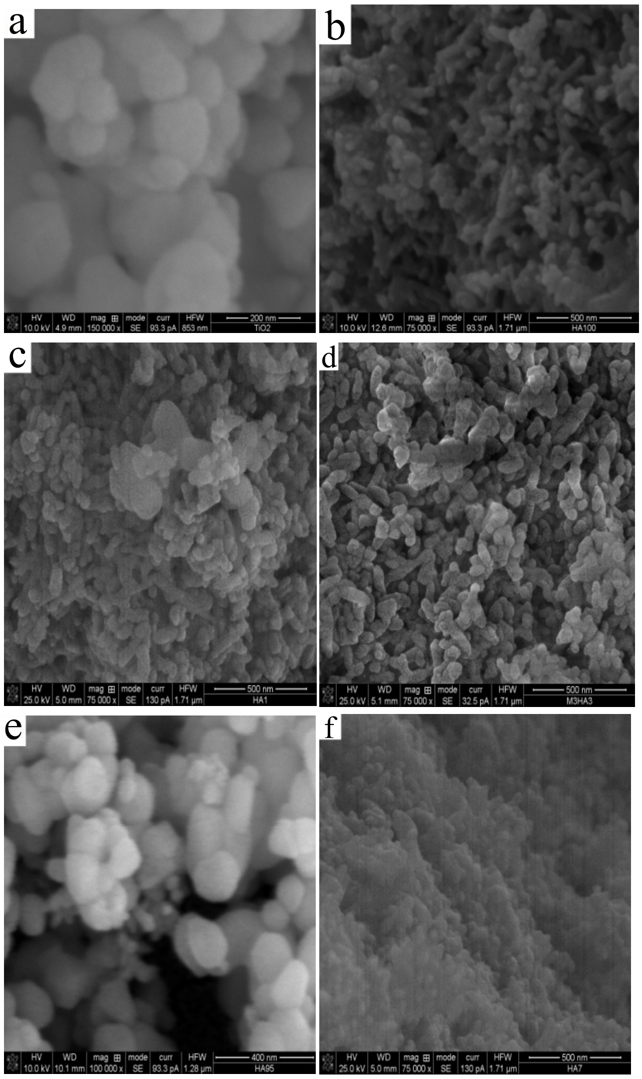

Figure 11: %HAcc + %TiO_2 micrographs SEM-HR show morphology changing. This changing begins at 5% and finishes at 7%.

alongside calcium. The nanometric size (hydroxyapatite and anatase) and crystal structure (hexagonal and tetragonal, respectively) play a fundamental role in the efficient dissemination of titanium into the network of HA. The nanometer HAcc wins elasticity but loses hardness (86%) compared to micro-HA.

Acknowledgement

Authors would like to thank Centro de Nanociencias y Micro y Nanotecnologías del IPN, Universidad Autónoma del Estado de Hidalgo and PhDs Prof. Heriberto Pfeifer, Martha Teresita Ochoa-Lara, Fidel Pérez-Moreno, Omar Novelo-Peralta, Carlos Flores-Morales, Luis Moreno-Ruiz, Mayahuel Ortega, Hugo Martínez, Juan Méndez-Méndez, Luis Lanturno-Rojas, José Andraca, Israel Arzate-Vazquez, Sc.M. Claudia Ramos-Torres, Jorge Osorio-Fuente, Ana Dueñas-Pérez, M.T.L. Muciño-Porras, Esteban Fregoso and Lidia Hernández-Hernández for their help and support in the characterization process.

Research Support

This work is partially financially by UNAM-IN109308, CONACyT 80380 projects.

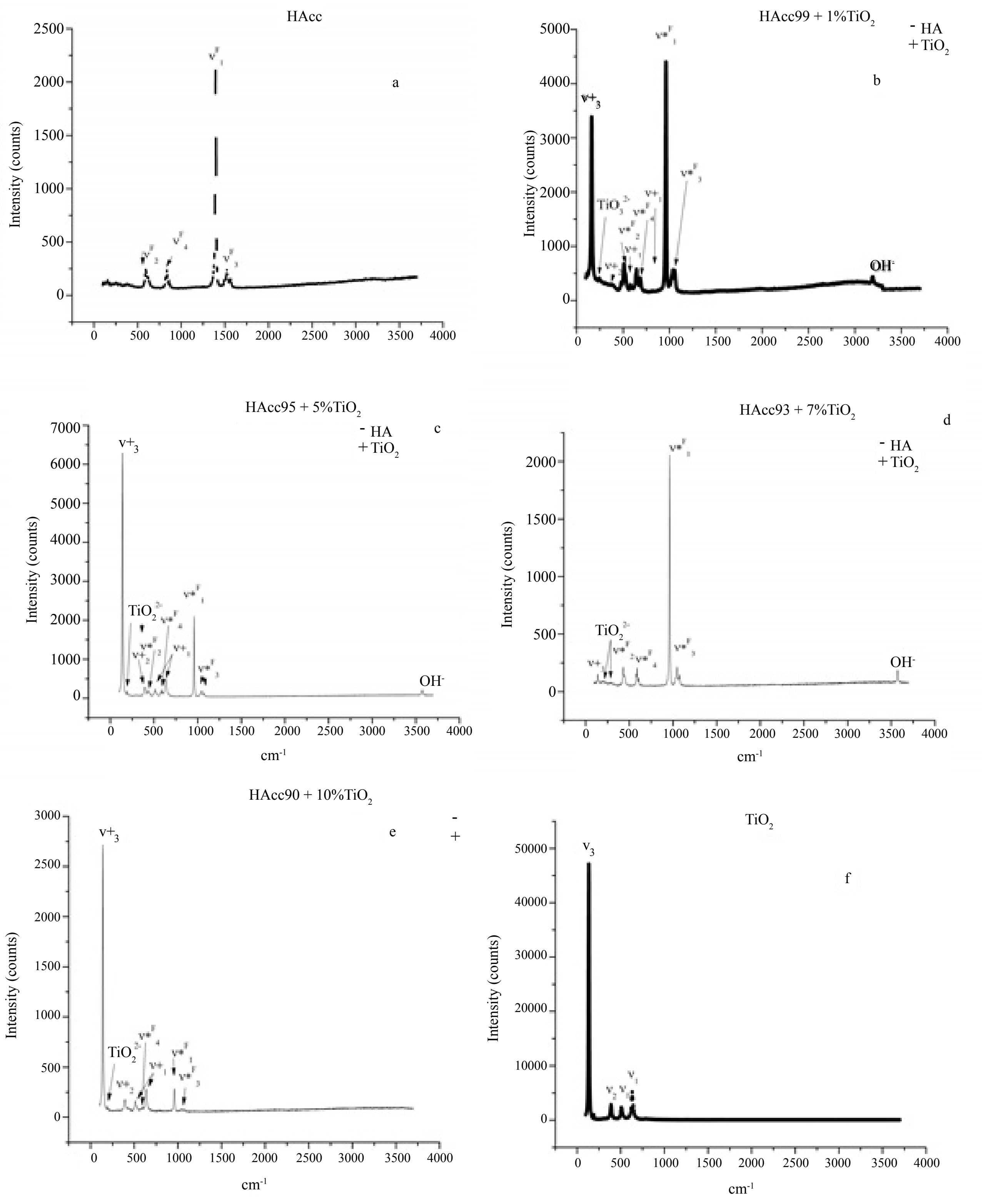

Figure 12: %HAcc + %TiO_2 Raman spectra show titanium spreading in HA matrix. This event begins at 5% and finished 7% of TiO_2.

Citation: Ledesma-Carrión DE (2016) Characterization and Effect of Anatase on Nano- Hydroxyapatite. J Bioengineer & Biomedical Sci 6: 189. doi:10.4172/2155-9538.1000189

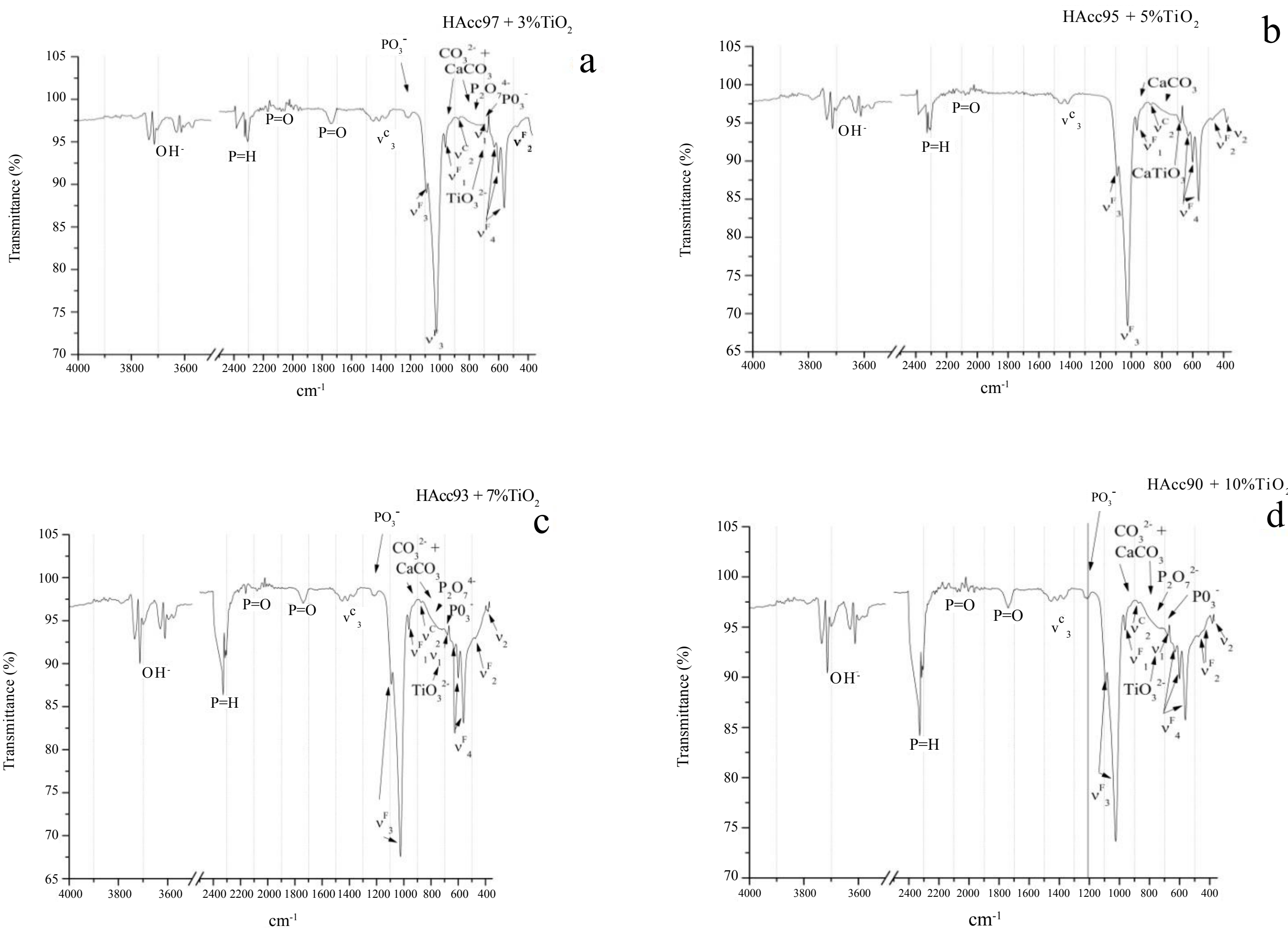

Figure 13: %HAcc + %TiO_2 IR spectra show that in 5% as stringer than others percentages.

HA+%TiO_2		Average nanoindentation parameters					
sample	%TiO_2	Hit [MPa]	Eit [GPa]	HV [vickers]	Welast [pJ]	Wplast [pJ]	Wtotal [pJ]
HAcc	0%	10861.7825 ± 19821.3121	182.6087 ± 297.1019	1005.9150 ± 1835.6637	11192.6071 ± 3934.5444	39647.6983 ± 17929.3067	50840.3058 ± 21561.5568
HA 99cc	1%	1651.6287 ± 615.3282	25.642 ± 5.6165	152.9575 ± 56.9867	23019.466 ± 5432.1530	48648.6413 ± 10871.5055	71668.1053 ± 10586.8408
HA97cc	3%	1614.936 ± 812.3526	32.3919 ± 9.6548	149.5621 ± 75.2337	18190.4433 ± 1505.5611	52840.02 ± 11248.1245	71030.4667 ± 11398.7152
HA95cc	5%	966.6493 ± 685.2454	30.5229 ± 11.0293	89.5233 ± 63.4623	15153.8233 ± 1553.1101	69711.5527 ± 23998.8906	84865.376 ± 24880.1465
HA93cc	7%	2074.1293 ± 3809.3971	54.9068 ± 79.3821	192.091 ± 352.8072	13441.668 ± 2431.6398	65936.578 ± 19415.1332	79378.2433 ± 21021.8409
HA90cc	10%	432.472 ± 151.8699	17.4101 ± 3.0183	40.0517 ± 14.0646	18323.8373 ± 1208.7926	118682.19 ± 16977.5081	137006.0273 ± 17289.4439

Table 3: Nanoindentation parameters before SBF.

HA+%TiO_2		Average nanoindentation parameters					
sample	%TiO_2	Hit [MPa]	Eit [GPa]	HV [vickers]	Welast [pJ]	Wplast [pJ]	Wtotal [pJ]
HAcc	0%	7971.9789 ± 20004.4035	70.868 ± 50.5837	738.2879 ± 1852.6095	15709.0584 ± 2708.4144	32336.7937 ± 17779.0402	48045.8516 ± 16574.0745
HA 99cc	1%	1973.4312 ± 520.769	26.927 ± 3.321	182.761 ± 48.229	23515.742 ± 2830.237	47297.730 ± 8603.547	70813.469 ± 8213.296
HA97cc	3%	2090.5815 ± 868.3384	43.71735 ± 9.3204	193.61155 ± 80.4172	15713.5 ± 1026.5850	45155.271 ± 12376.4190	60868.7685 ± 12275.2318
HA95cc	5%	1824.8085 ± 1744.0362	43.4206 ± 20.9334	168.9960 ± 161.5158	14207.309 ± 1130.2231	62104.081 ± 26317.3756	76311.3885 ± 25895.8589
HA93cc	7%	916.101 ± 599.7327	12.3915 ± 4.7685	84.8414 ± 55.5422	34992.4685 ± 4764.2556	85797.2465 ± 31177.6652	120789.717 ± 32705.3705
HA90cc	10%	1877.009 ± 2646.3581	31.8122 ± 21.1760	173.8311 ± 245.0781	18642.0865 ± 1703.0802	67980.0035 ± 32249.0934	86622.0905 ± 33030.2897

Table 4: Nanoindentation parameters after SBF 1 day.

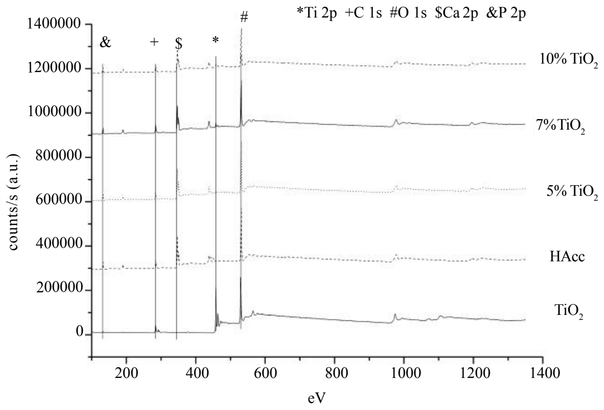

Figure 14: % HAcc + % TiO_2 XPS tests.

References

1. http://webmineral.com/data/Apatite-(CaOH).shtml
2. Piña MC, Munguía N, Palma R, Lima E (2006) Caracterización de hueso de bovino anorgánico: Nukbone. Acta Ortopédica Mexicana 20: 150-155.
3. Villora JM, Callejas P, Barba MF (2002) Métodos de síntesis y comportamiento térmico del hidroxiapatito. Boletin de la Sociedad Española de Cerámica y Vidrio 45: 443-450.
4. Kikuchi M, Itoh S, Ichinose S, Shinomiya K, Tanaka J (2001) Self-organization mechanism in a bone-like hydroxyapatite/collagen nanocomposite synthesized in vitro and its biological reaction in vivo. Biomaterials 22: 1705-1711.
5. Ali ANE, Mizoguchib T, Ito M, Bitar M, Salih V, et al. (2007) In vitro bioactivity and gene expression by cells cultured on titanium dioxide doped phosphate-based glasses. Biomaterials 28: 2967-2977.
6. Ledesma-Carrión DE (2015) Modification on the Synthesis Process of Hydroxyapatite. Asian Journal of Science and Technology 6: 1311-1315.
7. Ledesma-Carrión DE (2015) Nano-Hardness and Elasticity for Hydroxyapatite Before and After of Immersing It into Simulated Body Fluid. IJETST 2: 2704-2709.
8. Kumar RR, Wang M (2002) Functionally graded bioactive coatings of hydroxyapatite/titanium oxide composite system. Materials Letter 55: 133-137.
9. Fidancevska E, Ruseska G, Bossert J, Lin YM, Boccaccini AR (2007) Fabrication and characterization of bioce-ramic composites based based on hydroxyapatite and titania. Materials Chemistry and Physics 103:95-100.
10. Oyane A, Kim HM, Furuya T, Kokubo T, Miyazaki T, et al. (2003) Preparation and assessment of revised simulated body fluids. Journal of Biomedical Materials Research 65: 188-195.
11. García C, Paucar C, Gaviria J (2006) Study of some parameters that determine the synthesis of hydroxyapatite by the precipitation route. Dyna 73: 9-15.
12. Guzmán C, Piña C, Munguía N (2005) Stoichiometric hydroxyapatite obtained by precipitation and sol gel processes. Rev Mex Fis 51: 284-293.